THE JOURNAL OF BIOLOGICAL CHEMISTRY VOL. 285, NO. 3, pp. 2014–2027, January 15, 2010
© 2010 by The American Society for Biochemistry and Molecular Biology, Inc. Printed in the U.S.A.

Characterization of Chlorophenol 4-Monooxygenase (TftD) and NADH:FAD Oxidoreductase (TftC) of *Burkholderia cepacia* AC1100*[S]

Received for publication, August 14, 2009, and in revised form, November 11, 2009 Published, JBC Papers in Press, November 13, 2009, DOI 10.1074/jbc.M109.056135

Brian N. Webb[‡1], **Jordan W. Ballinger**[§1,2], **Eunjung Kim**[§3], **Sara M. Belchik**[§], **Ka-Sum Lam**[§], **Buhyun Youn**[§4], **Mark S. Nissen**[§], **Luying Xun**[§], **and ChulHee Kang**[‡§5]

From the [‡]*Department of Chemistry and* [§]*School of Molecular Biosciences, Washington State University, Pullman, Washington 99164-4660*

Burkholderia cepacia **AC1100 completely degrades 2,4,5-trichlorophenol, in which an $FADH_2$-dependent monooxygenase (TftD) and an NADH:FAD oxidoreductase (TftC) catalyze the initial steps. TftD oxidizes 2,4,5-trichlorophenol (2,4,5-TCP) to 2,5-dichloro-*p*-benzoquinone, which is chemically reduced to 2,5-dichloro-*p*-hydroquinone (2,5-DiCHQ). Then, TftD oxidizes the latter to 5-chloro-2-hydroxy-*p*-benzoquinone. In those processes, TftC provides all the required $FADH_2$. We have determined the crystal structures of dimeric TftC and tetrameric TftD at 2.0 and 2.5 Å resolution, respectively. The structure of TftC was similar to those of related flavin reductases. The stacked nicotinamide:isoalloxazine rings in TftC and sequential reaction kinetics suggest that the reduced FAD leaves TftC after NADH oxidation. The structure of TftD was also similar to the known structures of $FADH_2$-dependent monooxygenases. Its His-289 residue in the *re*-side of the isoalloxazine ring is within hydrogen bonding distance with a hydroxyl group of 2,5-DiCHQ. An H289A mutation resulted in the complete loss of activity toward 2,5-DiCHQ and a significant decrease in catalytic efficiency toward 2,4,5-TCP. Thus, His-289 plays different roles in the catalysis of 2,4,5-TCP and 2,5-DiCHQ. The results support that free $FADH_2$ is generated by TftC, and TftD uses $FADH_2$ to separately transform 2,4,5-TCP and 2,5-DiCHQ. Additional experimental data also support the diffusion of $FADH_2$ between TftC and TftD without direct physical interaction between the two enzymes.**

2,4,5-Trichlorophenol (2,4,5-TCP)[6] and 2,4,6-trichlorophenol (2,4,6-TCP) belong to an environmentally persistent class of contaminants known as polychlorinated phenols (1). They have been used extensively as pesticides and preservatives, particularly for lumber and leather preservation, and as general herbicides and biocides. Unfortunately, human exposure likely causes various adverse health effects (2). The concern has prompted governments worldwide to classify several polychlorinated phenols as priority pollutants.

Recently, two microorganisms that degrade trichlorophenols have been characterized. *Burkholderia cepacia* AC1100 mineralizes 2,4,5-TCP (3, 4), and *Cupriavidus necator* JMP134 completely degrades 2,4,6-TCP (5). 2,4,5-TCP 4-monooxygenase (TftD) of *B. cepacia* AC1100, an $FADH_2$-dependent monooxygenase, oxidizes 2,4,5-TCP to 2,5-dichloro-*p*-benzoquinone (2,5-DiCBQ), which is reduced to 2,5-dichloro-*p*-hydroquinone (2,5-DiCHQ) by NADH (Fig. 1*A*). TftD further oxidizes 2,5-DiCHQ to 5-chloro-2-hydroxy-*p*-benzoquinone, which is then reduced to 5-chloro-2-hydroxy-*p*-hydroquinone (5-Cl-2H-HQ) (6, 7). TftD can also oxidize 2,4,6-TCP to 2,6-DiCBQ but cannot further transform it or its reduced form 2,6-DiCHQ. In these reactions, TftD uses molecular oxygen and $FADH_2$ as co-substrates (8), and $FADH_2$ is supplied by TftC, a flavin reductase.

Several $FADH_2$-dependent monooxygenases, such as TftD, have been discovered in the biodegradation pathways of various aromatic compounds (9–12). The formation of a flavin-peroxide intermediate during catalysis has been proposed, and thus protection or stabilization of the FAD-peroxide intermediate from rapid hydrolysis seems crucial for those flavin-dependent monooxygenases (8, 13–16). All these monooxygenases have a small component as a partner, from which reduced flavins are provided. Those smaller reductases have a flavin molecule either as a tightly bound substrate or as a prosthetic group (10, 17–19). TftC and TftD belong to this two-component flavin-diffusible monooxygenase (TC-FDM) family and share se-

* This work was supported in part by National Science Foundation Grant MCB-0323167, the United States Department of Agriculture, Agricultural Research Service/Cooperative State Research, Education, and Extension Service, American Heart Association Grant 0850084Z, and The Murdock Charitable Trust.

[S] The on-line version of this article (available at http://www.jbc.org) contains supplemental Figs. 1–4.

The atomic coordinates and structure factors (codes 3K86, 3K87, 3K88, and 3HWC) have been deposited in the Protein Data Bank, Research Collaboratory for Structural Bioinformatics, Rutgers University, New Brunswick, NJ (http://www.rcsb.org/).

[1] Both authors contributed equally to this work.

[2] Present address: Hollister-Stier Laboratories, Spokane, WA 99207-5788.

[3] Present address: The Catholic University of Korea, Daejeon St. Mary's Hospital, Clinical Research Institute, Daejeon 300-824, Korea.

[4] Present address: Dept. of Biological Sciences, Pusan National University, Pusan 609-735, Korea.

[5] To whom correspondence should be addressed: School of Molecular Biosciences, Washington State University, Pullman, WA 99164-4660. Tel.: 509-335-1409; Fax: 509-335-9688; E-mail: chkang@wsu.edu.

[6] The abbreviations used are: 2,4,5-TCP, 2,4,5-trichlorophenol; 2,4,6-TCP, 2,4,6-trichlorophenol; TftD, chlorophenol 4-monooxygenase; TftC, NADH:FAD oxidoreductase; 2,5-DiCBQ, 2,5-dichloro-*p*-benzoquinone; 2,5-DiCHQ, 2,5-dichloro-*p*-hydroquinone; HpaB, 4-hydroxylphenylacetate 3-monooxygenase; MCAD, medium chain-specific acyl-CoA dehydrogenase; 4-BUDH, 4-hydroxybutyryl-CoA dehydratase; HPLC, high performance liquid chromatography; Mops, 4-morpholinepropanesulfonic acid; TCP, trichlorophenol; TC-FDM, two-component flavin-diffusible monooxygenase; MALLS, multiangle laser light scattering; ITC, isothermal titration calorimetry.

Downloaded from http://www.jbc.org/ at WASHBURN UNIVERSITY on March 3, 2015

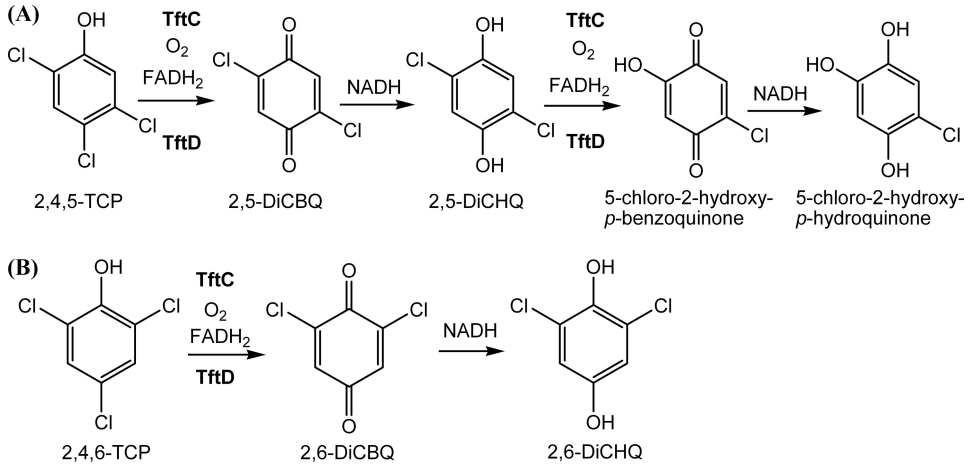

FIGURE 1. **2,4,5-TCP and 2,4,6-TCP oxidation by TftC and TftD.** *A*, TftD oxidizes 2,4,5-TCP to 2,5-DiCBQ, which is chemically reduced to 2,5-DiCHQ. Then, TftD oxidizes the latter to 5-chloro-2-hydroxy-*p*-benzoquinone, which can be nonenzymatically reduced to 5-chloro-2-hydroxy-*p*-hydroquinone. *B*, TftD also oxidizes 2,4,6-TCP to 2,6-DiCBQ but cannot further metabolize it. The latter is released and reduced to 2,6-DiCHQ. In these oxidation processes, TftC supplies $FADH_2$.

quence similarity with other flavin reductases and $FADH_2$-dependent monooxygenases that are involved in the degradation of various phenolic compounds.

So far, little is known about the interaction between TftC and TftD for $FADH_2$ transfer. Particularly reduced flavins can be readily oxidized by O_2 (20), and thus flavin dynamics is one of the critical features in the catalytic activity of monooxygenases. So far, several plausible mechanisms have been reported, *e.g.* (i) simple flavin diffusion between two components as in the cases of 4-hydroxyphenylacetate 3-monooxygenase of *Escherichia coli* and *Acinetobacter baumannii* (HpaB and HpaC) and phenol monooxygenase of *Bacillus thermoglucosidasius* (Phe-1(A) and Phe-2(A)) (21, 22); (ii) protein-protein interaction for direct substrate channeling as in the cases of bacterial luciferase (luciferase and flavin reductase P), alkane sulfonate monooxygenase (SsuE and SsuD), and arylamine oxygenase (PrnF and PrnD) (18, 23–26); and (iii) a probable combination of diffusion and complex formation for styrene monooxygenase (SMOA and SMOB) (27).

In addition, the dechlorination mechanism catalyzed by TftD is not well understood. An in-depth understanding of both TftC and TftD is important for elucidating the catalytic mechanisms, especially the mechanisms of sequential hydroxylations of 2,4,5-TCP. Here, we present a mechanistic analysis, including thermodynamic properties and crystal structures of TftC and TftD and propose a model for TCP oxidation. In addition, the plausible mechanism of flavin transfer between TftC and TftD was investigated through dynamic light scattering. This collective information could lead to the improvement of existing technologies for polychlorinated phenol bioremediation (28).

EXPERIMENTAL PROCEDURES

Plasmid Construction and Cloning—Both *tftC* and *tftD* were individually cloned into the overexpression plasmid pET30 LIC (Novagen) as described previously (8).

Expression and Purification—TftC or TftD expression was carried out by inoculating 100 ml of LB supplemented with 30 μg/ml kanamycin from a freezer stock of pET30TftC or pET30TftD in BL21(DE3) cells. This was allowed to grow overnight at 37 °C with constant shaking, after which this culture was used to inoculate 1.5 liters of LB medium. In addition, expression of selenomethionine-incorporated TftD in *E. coli* B834(DE3) (Novagen) was carried out using minimal media containing 30 mg/liter selenomethionine. Protein expression was induced by addition of isopropyl β-D-thiogalactopyranoside to a final concentration of 0.5 mM at mid-log phase growth (A_{600} = ~0.6). Following induction, the cells were incubated at 20 °C for 12 h with shaking at 250 rpm. Cells were harvested by centrifugation at 3,000 × *g*, and pellets were frozen to promote lysis. The cell pellet was then thawed at room temperature, resuspended in a minimal volume of lysis buffer (50 mM Tris (pH 8.0), 300 mM NaCl, and 20 mM imidazole for TftC, 20 mM Tris (pH 8.5), and 3 mM dithiothreitol in the case of TftD), sonicated 10 times for 10 s each using a model 450 Sonifier® (Branson Ultrasonics), and the resulting lysate cleared by centrifugation (20,000 × *g* for 40 min).

For the TftC purification, lysate was applied to a nickel-nitrilotriacetate column and washed with several column volumes of lysis buffer. Elution took place with the lysis buffer containing 300 mM imidazole. Eluted fractions containing TftC were combined, concentrated, and buffer-exchanged into 20 mM Tris (pH 8.5) containing 50 mM NaCl by ultrafiltration in an Amicon 8050 cell with a 30-kDa cutoff membrane (Millipore). TftC was then applied to an ion-exchange column (Bio-Rad Uno Q12), and the protein of interest was collected in the flow-through. TftC was then concentrated and added to several volumes of 5 mM sodium phosphate (pH 6.8). Precipitates formed during this step were removed by centrifugation, after which the remaining solution, containing only TftC, was concentrated and exchanged into 20 mM Tris (pH 7.5).

For the TftD purification, lysate was loaded onto an anion-exchange column (Toyopearl® DEAE 650 M) equilibrated with buffer A (flow rate 6.0 ml min^{-1}). TftD was eluted from the column using a linear NaCl gradient between 0 and 200 mM NaCl. TftD-containing fractions were desalted and concentrated into buffer B (5 mM sodium phosphate (pH 7.0)). Concentrated TftD was applied to a CHT-II hydroxyapatite column (Bio-Rad), equilibrated with buffer B (flow rate 2.0 ml min^{-1}), and eluted in the column flow-through. Fractions were then concentrated into buffer C (20 mM Tris (pH 7.0), 3 mM dithiothreitol), loaded onto a Mono Q™ GL10/100 anion-exchange column (GE Healthcare), and eluted with a linear NaCl gradient at ~300 mM NaCl. Fractions containing TftD were pooled, concentrated, and exchanged into buffer D (20 mM Tris (pH 7.0)), after which the protein was loaded onto a Sephacryl S-200 column (GE Healthcare) and separated from remaining proteins.

Downloaded from http://www.jbc.org/ at WASHBURN UNIVERSITY on March 3, 2015

With the exception of the nickel-nitrilotriacetate column, all purification steps were carried out using an Amersham Biosciences/BioCad 700E preparative HPLC (Applied Biosystems). All purification steps were monitored, and final homogeneity (>99%) was estimated using SDS-PAGE and Coomassie Blue staining.

Site-directed Mutagenesis and Enzyme Assay—Site-directed mutagenesis was performed using the QuikChange kit from Stratagene (La Jolla, CA). The primers used for the conversion of H289A of TftD are H289AF (5′-CGTATCTTCGACTGGGTGGCTTACCACATTTTGATCCG-3′) and H289AR (5′-CGGATCAAAATGTGGTAAGCCACCCAGTCGAAGATACG-3′). The mutations were confirmed by sequencing, and the correct clones were transformed into *E. coli* BL21(DE3) for protein production. The mutant protein (TftD H289A) was purified analogous to the wild-type protein for characterization. The enzyme activity was assayed as described previously (5). Briefly, 40 μl of assay mixture contained 20 mM potassium phosphate buffer (pH 7.0), 100 μM 2,4,6-trichlorophenol, 10 μM FAD, 300 μM NADH, 1 mM ascorbic acid, 0.1 μg/ml of *E. coli* flavin reductase (Fre), and various amounts of wild-type TftD or H289A mutant. The reaction was initiated by adding NADH to the reaction mixture and terminated by adding 40 μl of acetonitrile/acetic acid mixture (9:1 (v/v)). The samples were centrifuged at 13,000 $\times$ *g* for 2 min, and the supernatants were analyzed by HPLC (8). TftC enzyme kinetics were performed by adding FAD and NADH to the enzyme at the concentrations described and then monitoring the change in absorbance of NADH at 340 nm. K_m and V_{max} values were determined by fitting the data to the Michaelis-Menten equation using Origin 5.0.

Molecular Mass Determination—The weight-average molecular masses of TftC and TftD were measured by combined size exclusion chromatography and multiangle laser light scattering as described previously (29). Briefly, 100 μg of TftC (or TftD) was loaded onto a BioSep-SEC-S 2000 column (Phenomenex) and eluted isocratically with a flow rate of 0.5 ml min^{-1}. The eluate was passed through tandem UV detector (Gilson), Optilab DSP interferometric refractometer (Wyatt Technology), and a Dawn EOS laser light scattering detector (Wyatt Technology). Scattering data were analyzed using the Zimm fitting method with software (ASTRA) provided by the instrument manufacturer.

Dynamic Light Scattering—To test for the formation of a complex between TftC and TftD, we used a DynaPro Titan (Wyatt Technology Corp.). A scan was taken of each protein individually as well as a scan containing a mixture of TftC, TftD, FAD, and NADH. NADH was added just before each experiment, and FAD reduction was confirmed by a change in color of the mixture. Measurements consisted of 10 consecutive 5-s scans, and average molecular radius was measured using a Rayleigh sphere approximation. Data were analyzed using the manufacturer-supplied software, Dynamics 6.7.3.

Isothermal Titration Calorimetry—The heats of binding of TftC and TftD with various cofactors were measured with a VP-ITC Microcalorimeter (Microcal, Northampton, MA). For calorimetric measurements, TftC or TftD in 20 mM Mops (pH 7.2), 100 mM NaCl, 1 mM dithiothreitol was titrated with one of the substrates dissolved in the same buffer. The apo-form TftC, TftD, and substrate solutions were degassed prior to titration. The experiment consisted of 29 injections of 10 μl each of ligand into the protein solution at 25 °C with constant stirring at 300 rpm employing a 300-s equilibration interval between injections. Heats of dilution of each ligand were determined by titration of the ligand into buffer without protein and were used to correct the protein titration data. The Origin software package (OriginLab Corp, Northampton, MA) was used to fit the data to an *n*-sites equivalent binding model using nonlinear least squares regression. Fitting the data provides the affinity, enthalpy, and entropy change for the binding reaction.

Titrations of TftC with FAD, FMN, and NADH and titrations of TftD with FAD and FMN were performed under aerobic conditions. For TftD titration with $FADH_2$ and $FMNH_2$, the titration experiment was performed in a glovebox under anaerobic conditions. For anaerobic titrations, protein was diluted into buffer followed by addition of 1 mM NADH, 1 mM glucose, and 1 μg/ml catalase. The titrant was prepared under the same conditions but without TftD and with the addition of 100 μM flavin (FAD or FMN). The samples were degassed under vacuum and then placed in the glovebox. Glucose oxidase was added to 1 μg/ml to scavenge oxygen. The flavins were reduced by incubation with 1 μg/ml of *E. coli* flavin reductase (Fre), and the progress of the reaction was followed visually by the color change of the flavin.

Circular Dichroism—Experimental conditions for all CD measurements were 0.013 mg/ml protein in 20 mM sodium phosphate buffer (pH 6.8) at 25 °C. CD spectra were recorded from 200 to 300 nm using an AVIV 202SF spectrophotometer (AVIV Biomedical, Inc.).

Crystallization and Data Collection—Apo-form crystals of TftC were grown at 4 °C using the hanging drop vapor diffusion method. 1.5 μl of TftC in 20 mM Tris (pH 7.5) were mixed with 1.5 μl of reservoir solution (20% (w/v) polyethylene glycol 4000, 0.2 M potassium formate) and equilibrated against the reservoir. Crystals grew to a maximum size in 5 days and were of diffraction quality. For complex crystals of TftC with FAD and FAD·NADH, apo-form crystals of TftC were soaked for 6 and 3 h, respectively, by adding substrate directly to the drop containing the crystals.

Crystals of TftD were made by mixing 1.5 μl of protein solution (19 mg ml^{-1}) with an equal volume of crystallization solution (20% (w/v) polyethylene glycol 4000, 0.2 M $LiNO_3$ (pH 7.1)). The purified TftD protein lost its FAD during purification, and attempts to make a complex crystal were unsuccessful. Addition of the reducing agent prevented growth of TftD crystals and therefore was eliminated from the final (Sephacryl) purification step. Large single crystals grew slowly (over 1 month). Both crystals of TftC and TftD were flash-frozen by transferring to the cryoprotection solutions containing the corresponding reservoir solutions plus 20% glycerol. The intensity data were collected at the Advanced Light Source (ALS, BL 8.2.1) at 100 K and reduced and scaled using HKL2000 (30) and CrystalClear 1.3.6 (Rigaku/MSC).

Structure Determination and Refinement—Initial phasing of TftC data were done by the program AMoRe (31) through the coordinates of CobR (Protein Data Bank code 3CB0). Amino

Downloaded from http://www.jbc.org/ at WASHBURN UNIVERSITY on March 3, 2015

TABLE 1
Summary of crystallographic data

	TftD	TftC	TftC-FAD	TftC-FAD-NADH
Space group	$C222_1$	R3	R3	R3
Unit cell parameters				
a	148.20 Å	111.346 Å	111.529 Å	113.094 Å
b	149.87 Å			
c	212.01 Å	102.997 Å	102.523 Å	101.682 Å
Data	**Energy (λ)**	**Resolution (Å)**	**Completeness (%)**	**R_{merge}[a] (%)**
TftD phasing				
Edge	0.97956	25 to 2.5	99.8	5.5
Remote	0.91840	25 to 2.5	99.2	6.5
Peak	0.97934	25 to 2.5	99.5	6.7
Refinement	TftD	TftC	TftC-FAD	TftC-FAD-NADH
Resolution range	20 to 2.5 Å	20 to 2.0 Å	20 to 2.0 Å	20 to 2.0 Å
No. of reflections (>0)	79,750	31,822	25,673	27,350
Completeness	98.0% (97.0%)	98.9% (93.0%)	79.9% (72.0%)	83.6% (70.0%)
R_{work}[b]	0.17 (0.18)	0.15 (0.17)	0.16 (0.25)	0.16 (0.25)
R_{free}[c]	0.22 (0.25)	0.18 (0.21)	0.21 (0.30)	0.20 (0.30)
No. of atoms				
Nonsolvent	15,336	2,446	2,548	2,640
Solvent	1180	435	378	257
Wilson *B*-factor	22.6	23.2	25.2	27.8
Average *B*-value (Å^2)				
Nonsolvent	33.6	26.0	29.3	30.8
Solvent	33.8	40.7	42.7	41.6
r.m.s.d.[d]				
Bond lengths	0.004 Å	0.018 Å	0.016 Å	0.022 Å
Bond angles	0.757°	1.763°	1.737°	2.504°
Ramachandran plot[e]				
Favored	95.9%	98.5%	97.5%	97.5%
Allowed	99.1%	100%	100%	100%

[a] $R_{merge} = (\Sigma_h \Sigma_i |\langle F_h \rangle - F_{hi}|)/\Sigma_h F_h$, where $\langle F_h \rangle$ is the mean structure factor magnitude of *i* observations of symmetry-related reflections with Bragg index *h*.
[b] $R_{cryst} = \Sigma ||F_{obs}| - |F_{cal}||/|F_{obs}|$.
[c] R_{free} is calculated with removal of ≅5% of the data as the test set at the beginning of refinement.
[d] Root mean square deviations (r.m.s.d.) for main chain atoms are the root mean squared deviations of the bond lengths and bond angles from their respective ideal values as implemented in PHENIX.
[e] Ramachandran plots were created using the program MolProbity (51).

acid mutations were then performed using the graphics program O. Iterative model building and refinement took place using the programs O, X-PLOR, and PHENIX.

For TftD, location of the selenium heavy atom sites, phase calculation, and parameter refinement were performed using SOLVE (32) using a resolution range of 25 to 2.5 Å. This was followed by maximum-likelihood density modification using RESOLVE (32). After density modifications, well defined helical structures could be seen in the density, and the clear electron densities corresponding to most of the side chains allowed model building to proceed. The model was built into the electron density using the graphics program O (33) and refined using X-PLOR (34) and PHENIX (35). During the refinement processes for both TftD and TftC, the noncrystallographic symmetry restraint has not been applied. The final coordinates have been deposited in the Protein Data Bank as follows: apo-form TftC (3K86), FAD·TftC complex (3K87), FAD·NADH·TftC complex (3K88), and TftD (3HWC).

RESULTS

The apo-form of TftC was crystallized in the space group R3 with unit cell dimensions $a = b = 111.35$, $c = 103.00$ Å, and there were two TftC molecules in the asymmetric unit. Cell dimensions for the complex crystals of TftC were $a = b = 113.09$, $c = 101.68$ Å, and $a = b = 111.53$, $c = 102.52$ Å for FAD-NADH and FAD, respectively. TftD was crystallized in the space group $C222_1$, with cell dimensions of $a = 148.20$ Å, $b = 149.87$ Å, $c = 212.01$ Å, and four molecules in the asymmetric unit. A summary of the crystallographic data for both TftC and TftD is given in Table 1.

Structure of TftC—An asymmetric unit of the TftC crystal lattice contains a tightly associated homodimer, in which two subunits are arranged by the noncrystallographic C_2 axis. Each TftC subunit is composed of 4 α-helices and 12 β-strands. Most of those β-strands constitute a central twisted β-barrel, consisting of β2, β3, β4, β5, β6, β9, and β10, which is the core of each subunit. Two subunits are tightly assembled into a dimer by several interactions as follows: (i) the hydrophobic interaction between the 2-fold related side of each barrel; (ii) the α1 of each subunit is deeply embedded into the opposite subunit, corking its β-barrel; and (iii) a part of each β12 wraps around the β12 of the other subunit in an inter-subunit anti-parallel β-sheet. This dimeric nature of TftC in solution was confirmed by MALLS data (supplemental Fig. S1). The other side of the β-barrel is also corked by α2. Both α1 and α2 have an amphiphilic nature, and the hydrophobic sides of those two α-helices face toward the cavity of β-barrel, which is filled with hydrophobic residues. The overall structures of the apo-form and two complex structures showed no major differences in terms of their backbone structures. The Cα carbons among the apo-form and the complexes were superimposable with root mean square deviation values of 0.13 and 0.17 Å for the FAD complex and FAD·NADH complex, respectively.

As shown in supplemental Fig. S2, in addition to the N and C termini, three loop regions had elevated temperature factors as

Downloaded from http://www.jbc.org/ at WASHBURN UNIVERSITY on March 3, 2015

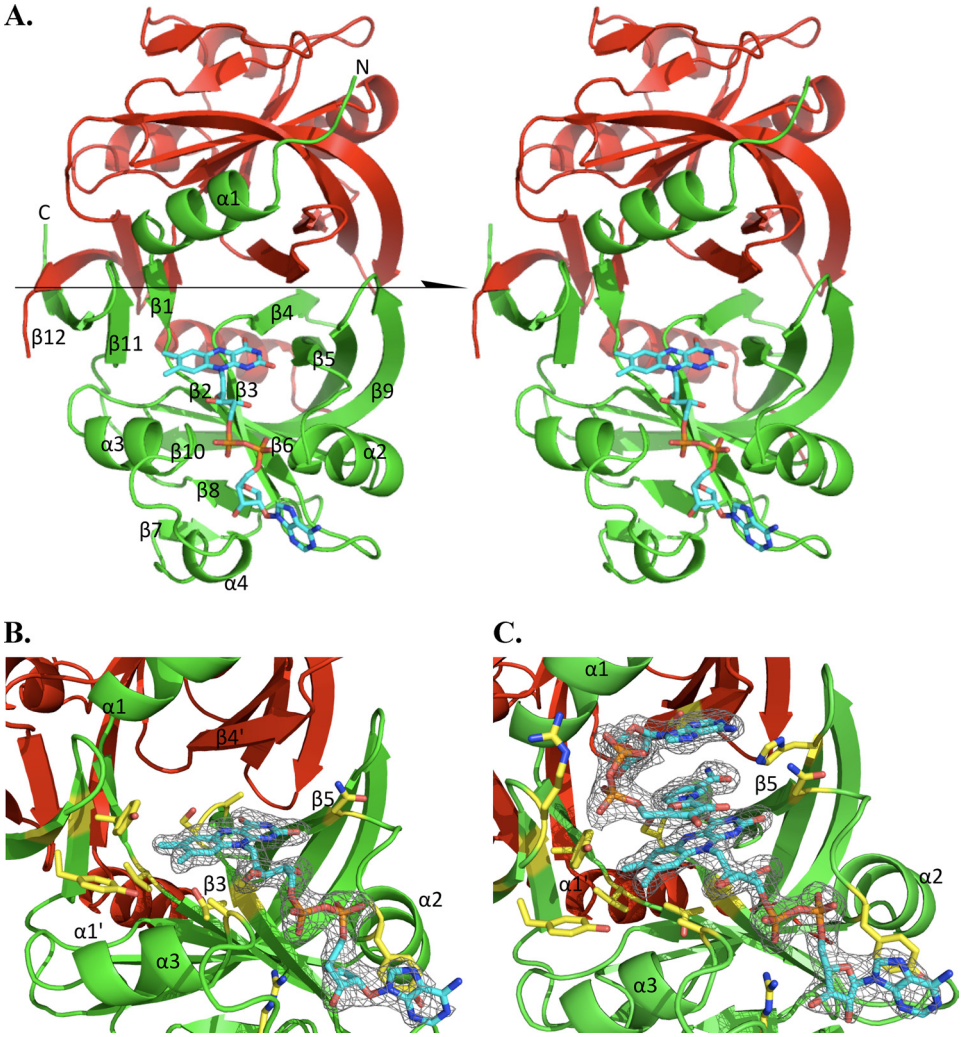

FIGURE 2. **Ribbon diagram representing the crystal structures of TftC and its binding site.** *A,* stereo view of the TftC dimer with associated FAD molecule with one subunit shown in *green* and the other in *red*. Secondary structural elements are labeled for one subunit and the noncrystallographic 2-fold axis is indicated by a *half-arrow*. *B,* difference map ($F_o - F_c$ map contoured at $\sigma = 1.0$) showed FAD molecule bound to TftC. Residues mentioned in the text as binding to the substrate are shown in *yellow*. *C,* difference map ($F_o - F_c$ map contoured at $\sigma = 1.0$) ternary complex of TftC showed both FAD and NADH. Residues important to substrate binding are shown in *yellow*. Several secondary structural elements near the FAD and NADH are labeled. Features marked with a *prime* are from the symmetry-related subunit. These figures were generated using Open-Source PyMOL™ (version 1.2).

follows: (i) between β5 and α2, (ii) between α3 and α4, and (iii) β10 and β11. As mentioned in detail later, the first and second loops among those three participate in coordinating an FAD molecule. Accordingly, the corresponding temperature factors for Asn-67, Tyr-71, Ala-99, and Val-104, which are located in those two loops (Fig. 3), were reduced significantly upon complex formation with FAD.

Substrate-binding Site of TftC—The $F_o - F_c$ maps of the FAD-soaked crystal data of TftC showed the corresponding electron density for the bound FAD molecule (Fig. 2*B*), with its isoalloxazine ring in a wide groove located at the dimer interface. The boundary of the binding pocket is made of α1, β1, β3, and β5 from one subunit and β4 of the other subunit. The isoalloxazine ring sits on top of antiparallel sheet made of β2, β3, and β6, facing its *re*-side toward the bulk solvent. The two FAD molecules in the homodimer have somewhat different conformations of their ribityl moieties, one adopting an extended conformation and the other a folded-back conformation. The corresponding quality and coverage of electron density for the extended conformation was similar to that of the folded-back site, but the extended confirmation can be superimposed well with that of FAD in the FAD·NADH complex structure. In addition, there is crystal packing potentially hindering a proper diffusion for the folded-back site. Therefore, only the extended form of FAD will be discussed. The O2 and O4 atoms of the isoalloxazine ring are hydrogen-bonded to backbone nitrogen atoms of Ala-51 and Asn-67. The N5 atom of the isoalloxazine ring is also hydrogen-bonded to the hydroxyl side chain of Ser-50. Among those, only the alanine residue is relatively conserved among seven related flavin reductases (Fig. 3). The dimethyl benzene moiety of the isoalloxazine ring is located in a pocket formed by residues Tyr-171, Tyr-166, and Val-33, all of which are highly conserved in all flavin reductases (Fig. 3). The pyrophosphate group of FAD is located between α2 and α3, which are in a perpendicular orientation with respect to each other. Its phosphate and ribose moieties form hydrogen bonds with Thr-48, Tyr-71, Ala-99, and Arg-109, among which only Arg-109 provides a side chain interaction.

The $F_o - F_c$ maps generated with the data collected from the crystal soaked with both FAD and NADH also clearly showed the corresponding electron density for both FAD and NAD(H) molecules stacked via the isoalloxazine and nicotinamide rings (Fig. 2*C*). In our FAD·NADH ternary complex of TftC, it is likely that the FAD molecules were in their reduced state judged by the pale yellow color of the soaked crystal in contrast to the intense yellow color of the FAD-containing crystal. The stacked isoalloxazine and nicotinamide rings were properly oriented at a distance of 3.5 Å between the C4 of NAD(H) and the N5 of FAD(H_2). The position of the FAD molecule in this FAD·NADH complex was superimposable with the FAD molecule in the FAD complex structure. The side chain of His-145 was within hydrogen bond distance with the amide group of nicotinamide, whose *re*-face (A-side) was facing the *re*-face of the isoalloxazine ring. The pyrophosphate group of NAD(H) was hydrogen-bonded through the backbone of Tyr-166 as well as the backbone and side chain of Arg-169. The N3A atom of the adenine ring is within hydrogen bonding dis-

Downloaded from http://www.jbc.org/ at WASHBURN UNIVERSITY on March 3, 2015

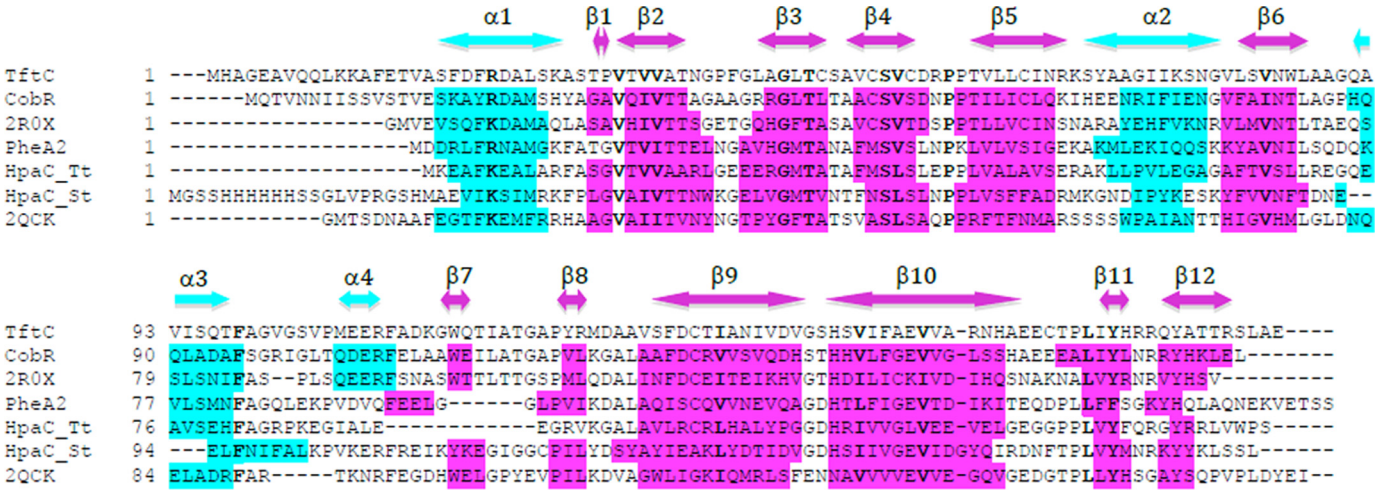

FIGURE 3. **Multiple sequence alignment between TftC and other flavin reductases.** The secondary structure of TftC is depicted using *arrows*, with *violet* indicating β-strands and *cyan* indicating α-helices. Secondary structure elements for all other sequences are highlighted using the same color scheme. Conserved residues are shown in *boldface*. *CobR*, corrin reductase from *B. melitensis*; *2R0X*, putative flavins reductase from *H. somnus* 129pt; *PheA2*, phenol 2-hydroxylase component B from *G. thermoglucosidasius*; *HpaC_Tt*, flavin reductase component of 4-hydroxyphenylacetate 3-monooxygenase from *T. thermophilus* hb8; *HpaC_St*, flavin reductase component of 4-hydroxyphenylacetate 3-monooxygenase from *S. tokodaii* str. 7; *2QCK*, flavin reductase domain protein from *Arthrobacter* sp. fb24.

tance from the hydroxyl group of Ser-54 from the other subunit. Significantly, all residues in the NAD(H)-binding site are highly conserved among all compared flavin reductases. Consequently, the coordination mechanism observed in TftC is almost identical to those of previously reported flavin reductases, including the folded NAD(H) confirmation, first reported for Phe-2(A), with a distance between the adenine C6 and nicotinamide C2 atoms of 4.4 Å.

Structure of TftD—Four tightly associated subunits in the crystal asymmetric unit are arranged in a noncrystallographic D_2 symmetric assembly (Fig. 4*B*). The tetrameric nature of TftD in solution was confirmed by the elution profile and molecular weight estimates from a MALLS experiment (supplemental Fig. S3). The individual TftD molecules consist of 14 β-strands and 17 α-helices (Fig. 4*A*) and can be divided into three sequential segments based on their constituent secondary structural elements. The first area from residues 1 to 146 is composed of seven α-helices (α1–α7) and four very short β-strands (β1–β4). The second area, which is composed of residues 147–273, has eight β-strands (β5–β12). The third area, C-terminal segment is composed of 10 (-helices (α8-α17) and 2 short β-strands (β13 and β14). Those three sequential segments are tightly interconnected in the three-dimensional structure. Noticeably, all of the 10 helices in the C-terminal segment, α8–α17, are involved in an inter-subunit interaction as discussed in detail later. All the eight β-strands in the second segment, β5–β12, are arranged in such a way as to appear almost like a β-barrel. At one side of this barrel, the β1 and β2 strands from the first segment fold back and together form a continuous β-sheet in the order of β2-β1-β10-β11-β7-β6 (Fig. 4*A*). The remaining four strands in the segment cover the other side of the same barrel in the order of β5-β8-β9-β12. The amino acid side chains of those 10 β-strands and the connecting loops between them form a hydrophobic core inside of the barrel.

Another noticeable structural feature is that three long α-helices, α9, α10, and α11, and three short helices, α14, α15, and α16, which are all from the C-terminal segment, form a sizeable helix bundle together with two short α-helices from the first segment, α4 and α5. The surfaces of most of those α-helices are mostly hydrophobic, establishing a hydrophobic interaction among them.

The corresponding electron densities for the C-terminal residues 442–445 and 483–515 are not visible, probably due to being disordered. In addition to the immediate neighbors of these two regions, the temperature factors for residues 158–167, which form an exposed loop connecting β5 and β6, showed higher temperature factors than the rest of the molecule.

The observed tetramer interface had an extensive network of inter-subunit interaction among the C-terminal α-helices. In particular, α16 and α17 extend out of the individual subunit to embed themselves into the hydrophobic surface made by α9, α10, and α14 of the adjacent subunit. In addition, a large portion of two anti-parallel C-terminal helices, α10 and α11, from two neighboring subunits contact closely in a perpendicular orientation generating a substantial hydrophobic interface between subunits. These hydrophobic interfaces involve residues such as Val-326, Leu-334, Leu-360, Phe-364, Leu-450, Phe-454, and Met-458. The remaining three α-helices at the C-terminal segment also form another type of subunit interaction together with the above-mentioned β-barrel-like motif, *i.e.* α12, α13, α15, their connecting loops, and the surface-exposed residues in one side of the barrel form a tightly associated noncrystallographic 2-fold related interface. This interface also possesses tightly packed hydrophobic residues as follows: Val-187, Val-190, Phe-230, Val-257, Leu-389, Met-398, Trp-405, and Phe-406. However, contrary to the above-mentioned hydrophobic interface involving α16 and α17, a substantial amount of polar inter-subunit interaction was observed, which includes Asp-159, Glu-233, Lys-237, Asp-250, Asp-259, Arg-386, Gln-396, Gln-401, Asn-410, Arg-420, Arg-428, Asp-434, and Arg-438.

Downloaded from http://www.jbc.org/ at WASHBURN UNIVERSITY on March 3, 2015

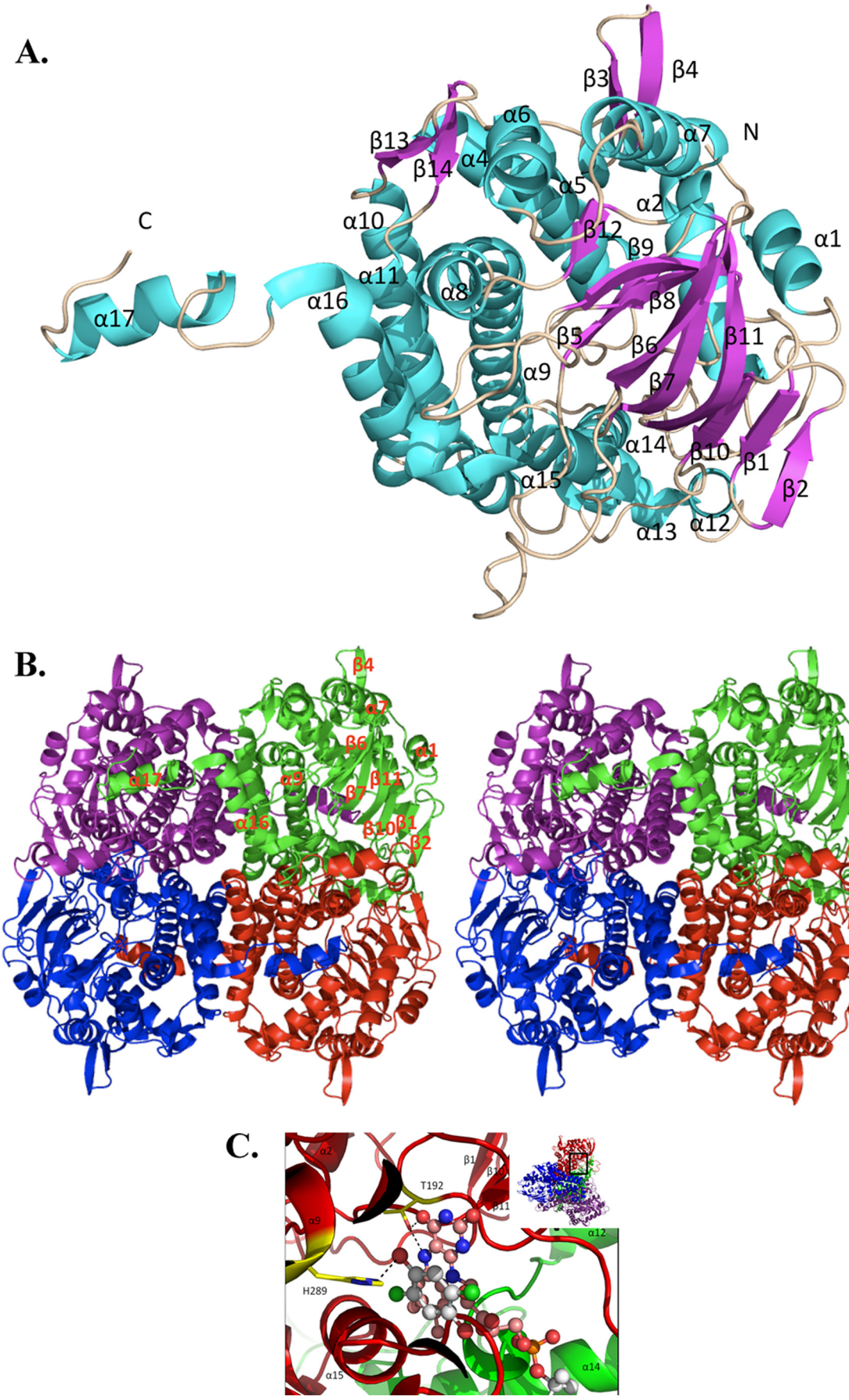

Downloaded from http://www.jbc.org/ at WASHBURN UNIVERSITY on March 3, 2015

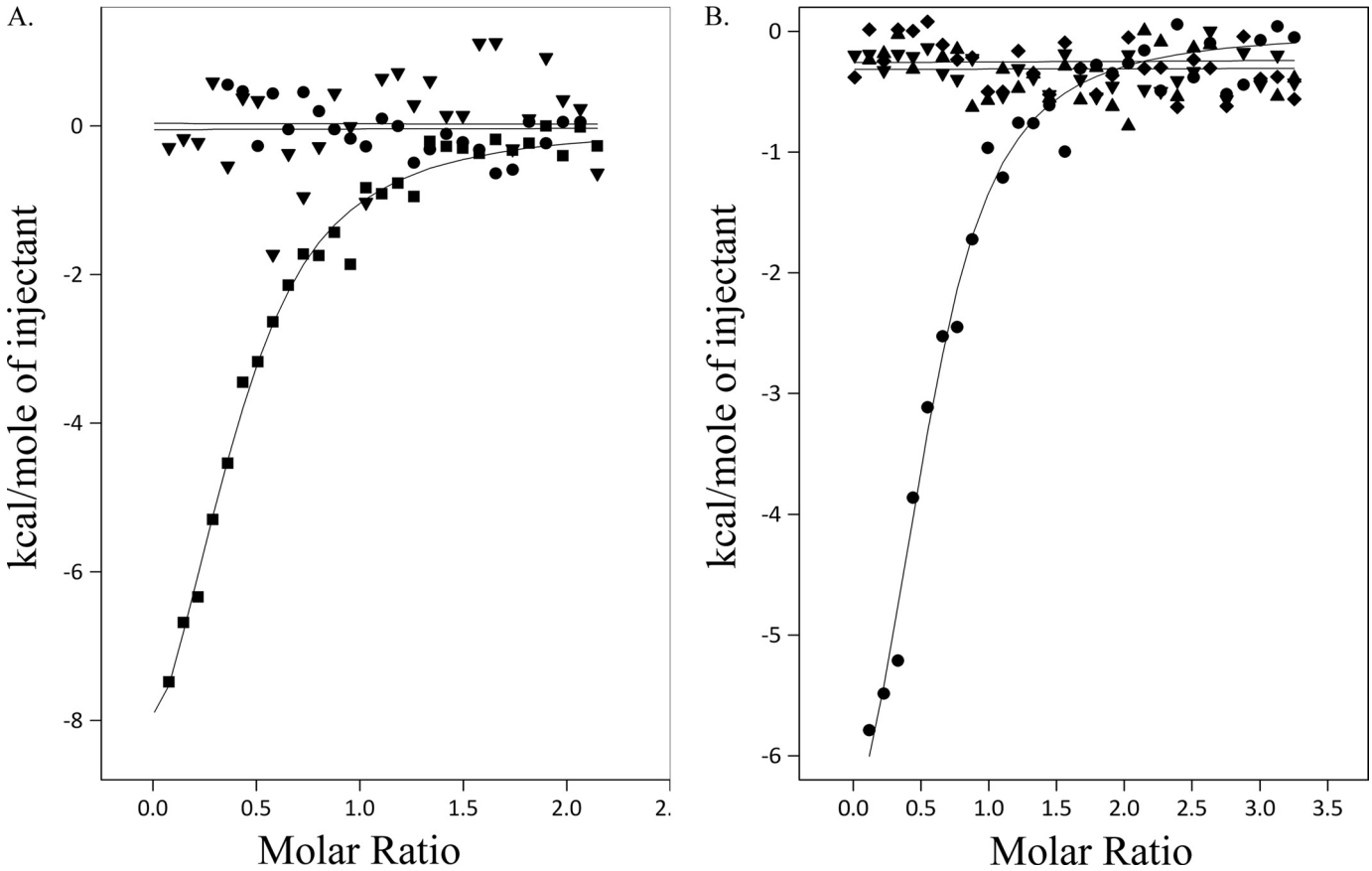

FIGURE 5. **Measurement of substrate binding through ITC experiments.** *A,* trend of heat released by serial injections of FAD (*square*), FMN (*inverted triangle*), or NADH (*circle*) into apo-form TftC was monitored. Only FAD showed the typical heat-release pattern indicative of binding. *Solid lines* represent the least square fits of the data using a single-site binding model. *B,* injections of FAD (*diamond*), FMN (*triangle*), $FADH_2$ (*circle*), and $FMNH_2$ (*inverted triangle*) into apo-form TftD.

Substrate-binding Site of TftD—In the apo-structure of TftD, a unique entry site and binding pocket for $FADH_2$ was clearly distinguishable (Fig. 4*C*). The perimeter of this widely open entry site is made with three flexible loops as follows: (i) between β5 and β6, (ii) between β8 and β9, and (iii) between α15 and α16. Among those three, the first and third loops have high temperature factors and show the most heterogeneous conformations among the four subunits, reflecting their high level of flexibility. The residues lining this entry site are predominantly hydrophilic, and a few ordered solvent molecules were located in the entry site of the determined apo-form structure of TftD.

The position of the riboflavin moiety of the $FADH_2$ was readily obtained through the combination of superposition with the 4-hydroxyphenylacetate 3-monooxygenase (HpaB) from *Thermus thermophilus* HB8 (2YYJ) (36) and the solid docking module on Quanta (BioSYM/MSI, Inc.), which is based on conformational space, followed by a quick energy minimization by CNS version 1.1 (37). The wall of this binding pocket is made with small portions from β5, β7, β8, β11, α9, and α15 of one subunit and portions of α9, α10, and α11 of another subunit.

Isothermal Titration Calorimetry (ITC) for TftC and TftD—ITC was used to characterize the binding of FAD, FMN, and NADH to TftC. As shown in Fig. 5*A*, a significant amount of heat is released when TftC is titrated with FAD. However, a negligible amount of heat was released when TftC was titrated with FMN and NADH, indicating a lack of binding. A calculated K_d of FAD is 1.8 $\pm$ 0.1 μM (mean $\pm$ S.D.), with a large enthalpic contribution ($\Delta H = -11.5$ kcal/mol). The data also indicated an unfavorable entropic contribution, with a calculated ΔS of -12.29 cal/mol/degree, possibly indicating that the TftC structure was slightly stabilized upon binding of FAD, and very few solvent molecules were freed from the pocket. These thermodynamic data were consistent with structural data, as indicated by the significant reduction of the *B*-values for two loops constituting the binding pocket upon formation of the FAD binary complex. There were few solvent molecules in the FAD binding pocket.

FIGURE 4. *A,* ribbon diagram representing the crystal structure of TftD subunit. Secondary structure elements have been numbered sequentially as α1–α17 and β1–β14 following the convention. *N* and *C* refer to N- and C-terminal regions, respectively. β-Strands are shown in *magenta,* and α-helices are shown in *cyan*. The subunit orientation is analogous to that of the *green* subunit in *B* for reference. *B,* arrangements of the tetrameric TftD in a noncrystallographic D_2 symmetry. A few secondary structural elements have been labeled as a guide. *C,* structure of the substrate-binding pocket of TftD with FAD and 2,5-DiCHQ. The participating residues in binding 2,5-DiCHQ and FAD are shown with their residue numbers and *lines* representing hydrogen bonds. The chlorine atoms in 2,5-DiCHQ has been depicted in *green*. These figures were generated using Open-Source PyMOL™ (version 1.2).

Downloaded from http://www.jbc.org/ at WASHBURN UNIVERSITY on March 3, 2015

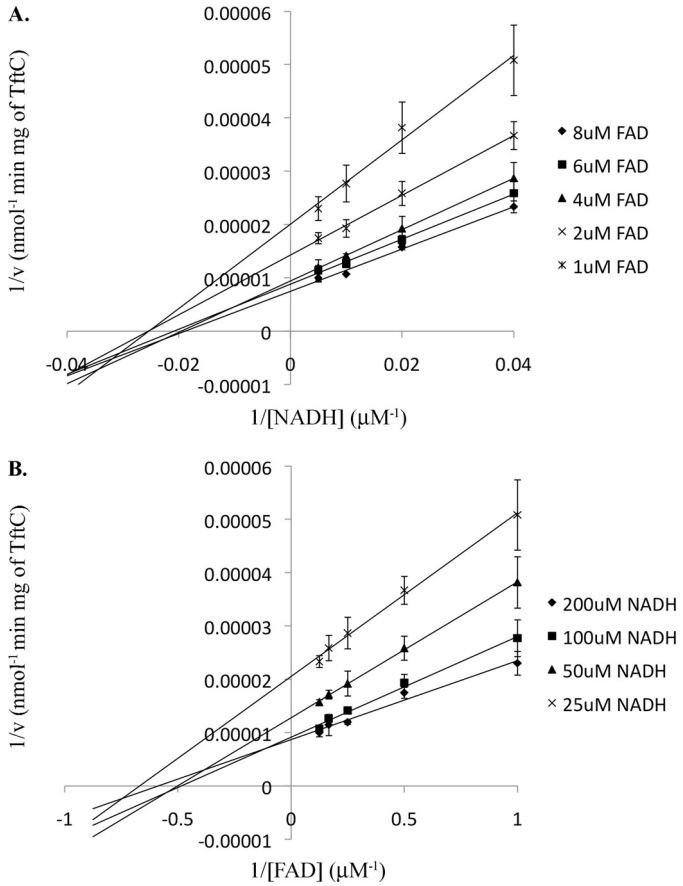

FIGURE 6. **Kinetic analysis of TftC.** Double-reciprocal plots of initial velocities of TftC *versus* substrate concentration. *A,* each *line* represents an experiment with a constant concentration of FAD, whereas the concentration of NADH is varied. *B,* each *line* is an experiment in which NADH was held constant while varying FAD concentration. The double-reciprocal plot yielded lines intersecting to the *left* of the *y* axis, indicating a sequential reaction mechanism. *Error bars* indicate 1 S.D.

As in the case of TftC, ITC was used to confirm the differential binding affinities of FAD and FMN for TftD and their corresponding reduced forms. As shown in Fig. 5*B*, FAD, FMN, and $FMNH_2$ molecules did not show any significant binding to TftD. However, a significant amount of heat was released when $FADH_2$ associated with TftD, indicating that the binding interactions had significant enthalpic contributions ($\Delta H = -8.33$ kcal/mol). The data also showed a slightly unfavorable entropic contribution ($\Delta S = -0.78$ cal/mol/degree); however, it is less significant than ΔS of TftC. ITC data analysis yielded a K_d for $FADH_2$ binding to TftD of 1.2 ± 0.2 μM.

Enzyme Kinetics and Site-directed Mutagenesis—Steady-state kinetics experiments were performed by holding the concentration of TftC constant while varying the FAD concentration at 1, 2, 4, 6, and 8 μM. The NADH concentrations in the corresponding four experiments were varied at 25, 50, 100, and 200 μM, and each point was performed in triplicate. As shown in Fig. 6, the double-reciprocal plot of the inverse rate *versus* inverse substrate concentration yielded lines intersecting to the left of the *y* axis, indicating a sequential reaction mechanism. The calculated K_m values for FAD and NADH were 2.0 (±0.3) and 45.3 (±4.5) μM, respectively. The V_{max} value was 120.3 (±7.7) μmol min^{-1} mg^{-1}.

TABLE 2
Kinetic properties of TftD and TftD H289A

	K_m	k_{cat}	k_{cat}/K_m
	μM	s^{-1}	M^{-1} s^{-1}
2,4,5-TCP			
TftD[a]	35.8 ± 3.9	0.67 ± 0.03	1.9×10^4
TftD H289A	36.6 ± 3.4	0.024 ± 0.003	6.6×10^2
2,4,6-TCP		(28 times)	
TftD[a]	39.9 ± 7.6	0.41 ± 0.03	1.0×10^4
TftD H289A	18.5 ± 2.4	0.0078 ± 0.0006	4.2×10^2
2,5-DiCHQ		(53 times)	
TftD[a]	4.3 ± 1.1	0.10 ± 0.01	2.3×10^4
TftD H289A[b]		0	

[a] Experiments were done in 40 mM KP_i buffer (pH 7.0) at 24 °C. Values are means of triplicate experiments with standard deviations. The kinetic properties of TftD were reported previously (8).
[b] No activities.

As discussed under "Discussion," the structure of TftD indicated that one of the residues in the active site, His-289, might play a critical role in its catalysis, and thus TftD H289A mutant enzyme was generated, and its structural integrity was compared with that of the wild type by measuring their CD spectra. As shown in the supplemental Fig. S4*A*, the spectral pattern of H289A mutant in a buffer containing 20 mM sodium phosphate (pH 6.8) was superimposable to that of the wild type. Both have two negative bands around 208 and 222 nm, which are the characteristics of CD spectra of typical α-rich or αβ proteins. The tetrameric nature of the H289A mutant in solution was also confirmed by a MALLS experiment (supplemental Fig. S4*B*). The enzyme activities for the mutant were assayed using 2,4,6-TCP, 2,4,5-TCP, or 2,5-DiCHQ as the substrate. TftD H289A mutant still used 2,4,5-TCP and 2,4,6-TCP as substrates with about 28- and 53-fold decreases in k_{cat}, respectively, and the K_m values were not significantly altered (Table 2). Most significantly, the mutant enzyme completely lost activity toward 2,5-DiCHQ.

Dynamic Light Scattering—To probe the dynamics of flavin transfer between the small component flavin reductase and the large component monooxygenase, chemical cross-linking and dynamic light scattering were employed. The average Rayleigh sphere radius of TftC and TftD was measured independently and in combination with TftC substrates. When a solution of TftC and TftD (also containing FAD and NADH) was measured, FAD was reduced to $FADH_2$. As was confirmed by the color change and the FADHOOH spectrum (8), the bound $FADH_2$ in TftD was immediately oxidized to FADHOOH. Thus, most added FAD is in the form of the FADHOOH·TftD complex. If a higher order complex were formed between the two enzymes to transfer $FADH_2$, the height of the TftC peak would either decrease or disappear, whereas the TftD peak would appear to shift to a larger radius. As Fig. 7 indicates, addition of substrates (FAD and NADH) causes no significant shift in intensity or any shift in average particle size, indicating a lack of interaction between the two enzymes. Similar experiments were carried out using chemical cross-linking, and the results indicated the same outcome (data not shown). This supports the growing body of evidence that flavin transfer in TC-FDM systems occurs via a purely diffusive mechanism (21, 38, 39).

Downloaded from http://www.jbc.org/ at WASHBURN UNIVERSITY on March 3, 2015

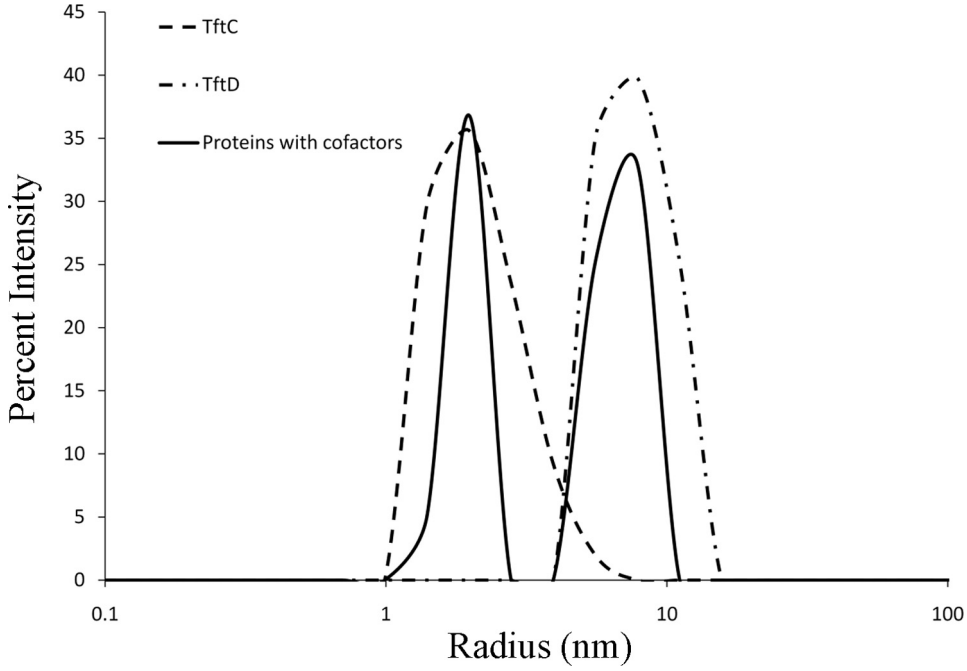

FIGURE 7. **Dynamic light scattering analysis.** Dynamic light scattering was used to probe for physical interaction between TftC and TftD during reduced flavin transfer. TftC is the *dashed line*; TftD is the *dash/dot line*, and a mixture of the two proteins with FAD and NADH is shown as a *solid line*. The plot indicates a lack of physical interaction between the two proteins, indicating the reduced flavin could transfer via a diffusive mechanism.

DISCUSSION

We have determined the crystal structures of both TftC and TftD to shed light on their reaction mechanism and structural relationship to other flavin-dependent monooxygenases and flavin reductases in TC-FDM. In particular, TftC and TftD together perform two sequential oxidative dechlorination steps in the degradation process of 2,4,5-TCP (Fig. 1) (8), even though most monooxygenases hydroxylate their substrate only once (40, 41). For TftC, in addition to its apo-form, structures of the binary complex with FAD and the ternary complex with FAD and NADH were also determined. However, we were unable to produce a complex crystal of TftD with FAD under aerobic environments, likely due to the negligible affinity of TftD for FAD as shown by our ITC data (Fig. 5*B*). Consequently, the position of flavin was determined through superimposition with structural homologues and a substrate docking approach.

Structural Classification for TftC

The primary and tertiary structural comparison of TftC revealed its high similarity with other flavin reductases. A Dali search showed that the most similar structure was corrin reductase (CobR) from *Brucella melitensis* (3CB0) with a high *Z*-score of 33.5, followed by putative flavin reductase from *Haemophilus somnus* (2R0X) with a *Z*-score of 26.3, Phe-2(A) from *Geobacillus thermoglucosidasius* (1RZ1) with 23.3, HpaC from *Sulfolobus tokodaii* str. 7 (2D37) with 21.8, and HpaC from *T. thermophilus* (2ECR) with 21.0. In general, the β-barrel-like core structure and dimeric nature of TftC are similar to the structures of high similarity scores, which include other small component members of the TC-FDM family, such as Phe-2(A), $HpaC_{St}$, and $HpaC_{Tt}$. However, a detailed visual inspection revealed a structural heterogeneity in terms of the number and size of helices in the peripheral regions. Additionally, the C terminus of each TftC subunit forms interlocking anti-parallel β-strands with each other, which has not been observed in other flavin reductases. Noticeably the structure of TftC is quite different from that of EmoB, which is also a small component of TC-FDM (19). A search for similar amino acid sequences in the Protein Data Bank using BLAST (42) revealed that putative flavin reductase from *H. somnus* (2R0X) and CobR (3CB0) showed the highest score (119 bits) with 40 and 38% identity among matched amino acids to TftC, respectively, followed by Phe-2(A) (1RZ0, 70.5 bits, 31% identity), $HpaC_{St}$ (2D36; 57.4 bits, 25% identity), and $HpaC_{Tt}$ (2ECR; 56.6 bits, 26% identity). The conserved residues were distributed sporadically through the entire secondary structural elements. The α2 and its neighboring loops show the least similarity among the above reductases (Fig. 3). In addition, there are insertions or deletions between α3 and β7 producing heterogeneity in the secondary structural elements among those compared flavin reductases. Significantly, this area of heterogeneity happens to be involved in binding of the adenine moiety of flavin in those reductases. In Phe-2(A) and $HpaC_{Tt}$, binding for the adenine moiety is through multiple hydrogen bonds with this region referred to as Loop 7. However, as noted previously in the structure of CobR (43), Loop 7 is replaced by an additional α-helix, α4, in TftC, which alters the binding interactions with AMP. It should also be noted that HpaC of *S. tokodaii*, which prefers FMN to FAD, contains a 3_{10} helix in the same position as α4 in TftC.

The residues constituting the hydrophobic binding pocket for the dimethyl benzene moiety of the isoalloxazine ring are highly conserved among those enzymes. However, the corresponding sites facing the 2,4-pyridine side and the ribose group of the flavin molecule are not well conserved among the structurally related proteins (Fig. 3). Despite this poor sequence similarity, the backbones of the corresponding regions are similarly engaged in coordination in all the compared reductases whose complex structures are available.

Structural Classification for TftD

A Dali search was also used for identifying structural homologues for TftD (45) and showed that the highest match was to the 4-hydroxyphenylacetate 3-monooxygenase (HpaB) of *T. thermophilus* HB8 (2YYL) (36) with a *Z*-score of 43.7. It was followed by 4-hydroxybutyryl-CoA dehydratase (4-BUDH) of *Clostridium aminobutyricum* (1U8V) (46) with a *Z*-score of 36.5 and a couple of other structural homologues with much

Downloaded from http://www.jbc.org/ at WASHBURN UNIVERSITY on March 3, 2015

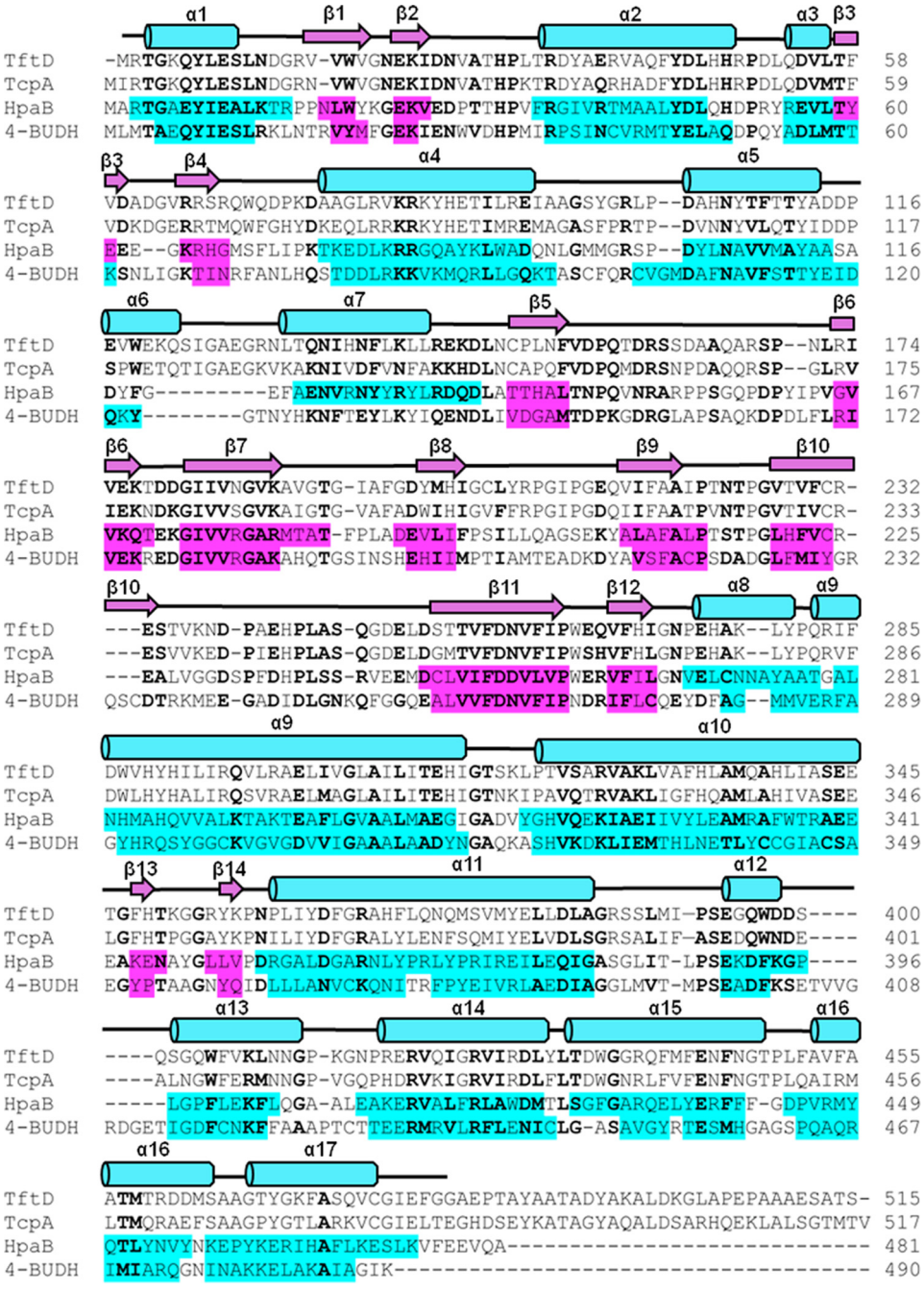

FIGURE 8. **Amino acid sequence and secondary structure alignment of TftD with other flavin-dependent monooxygenases.** Secondary structure elements for TftD are depicted as *violet arrows* and *cyan cylinders* for β-strands and α-helices, respectively. Secondary structural elements for HpaB and 4-BUDH are also highlighted in colors (*violet* for β-strands and *cyan* for α-helices). Conserved residues among those monooxygenases are shown in *boldface*. TcpA, 2,4,6-trichlorophenol monooxygenase from *Cupriavidus necator* JMP134; HpaB, 4-hydroxyphenylacetate 3-monooxygenase from *T. thermophilus* HB8; *4-BUDH*, 4-hydroxybutyryl-CoA dehydratase from *C. aminobutyricum*.

lower *Z*-scores such as medium chain-specific acyl-CoA dehydrogenase (MCAD) from pig mitochondria (3MDE) (47). Careful manual comparisons of these crystal structures show that they share similarity with TftD in terms of the location of secondary structural elements and topological connectivity (Fig. 8). Consistent with a structural similarity among TftD, MACD, HpaB, and 4-BUDH, there is significant sequence similarity among these structural homologues. For example, TftD and HpaB share 28% identity and 48% similarity in their amino acid sequences. However, there were also significant structural differences among them. For example, in HpaB, the α6 is missing due to a major deletion near that region (Fig. 8).

Substrate-binding Site and Reaction Mechanism

TftC—The observed conformation of the AMP moiety of the bound FAD in TftC is quite different from that in the complex crystal of the Phe-2(A) and HpaC; likewise, the local conformation of TftC shows difference from those, *i.e.* the exposed adenine ring of the FAD stacks with the phenyl side chain of tyrosine 71 in the TftC structure, in contrast to the definite binding pocket offering multiple hydrogen bonds to the adenine ring observed in both Phe-2(A) and HpaC. This apparent difference in binding of the AMP moiety of FAD might result in a lower affinity for FAD (K_d = 1.8 μM) and loss of FAD during the purification. In addition, there was no flavin occupancy in the apo-form crystal structure. This is in contrast with what has seen in other flavin reductases, such as Phe-2(A), which has a nanomolar affinity for flavin.

The NADH:FAD oxidoreductase activity of TftC was through oxidation of an NADH molecule by a bound FAD molecule, which caused reduction of the flavin. The ternary complex structure of TftC showed that the stacked nicotinamide: isoalloxazine rings were at a proper distance for hydride transfer. Compared with the FAD molecule, the NAD(H) molecule in the ternary complex of TftC had less interaction with the enzyme despite its interactions with highly conserved residues and many water-mediated interactions, which are very similar to that of Phe-2(A). The NAD(H) molecule had a negligible affinity with TftC that had no bound FAD in it, as indicated by the ITC results (Fig. 5*A*). Therefore, the apparent affinity for NADH existed only after the FAD occupies its site in TftC. In addition, in the crystal structure for the FAD·NADH ternary complex form, the adenine ring is folded back in a stacking position on top of the nicotinamide ring, probably shielding the

Downloaded from http://www.jbc.org/ at WASHBURN UNIVERSITY on March 3, 2015

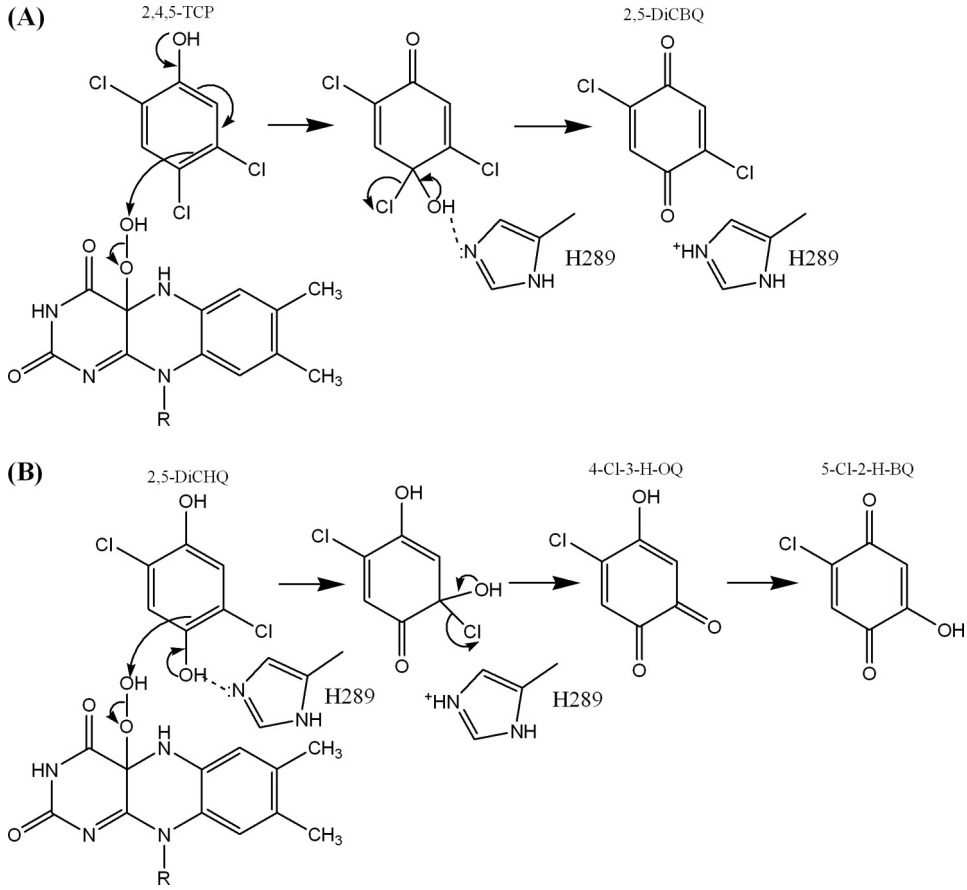

FIGURE 9. **Proposed reaction mechanism in the active site of TftD.** *A,* 2,4,5-TCP as a substrate; *B,* 2,5-DiCHQ as a substrate. In both cases, His-289 acts as a general base. The *arrows* indicate the movement of an electron. The figures were made using ChemBioDraw Ultra 11.0 (Cambridge Corp.).

C4 atom of nicotinamide from bulk solvent (Fig. 2*C*). This is also observed in both HpaC and Phe-2(A) structures (48), allowing the efficient hydride transfer to FAD. Once FAD in TftC is reduced by NADH, the FAD molecule will leave as $FADH_2$. Based on the results from the double-reciprocal plot, it is obvious that the production of $FADH_2$ by TftC is through a sequential reaction mechanism (Fig. 6). In the catalytic cycle NADH reduces the associated FAD and NAD^+ leaves TftC. The diffusible $FADH_2$ is then used by TftD for TCP metabolism. In this process, the NADH molecule delivers its hydride through transiently stacked interactions of its nicotinamide ring with the isoalloxazine ring of FAD as similarly observed in the complex structures of EmoB, Phe-2(A), and HpaC (19, 44, 48, 49).

TftD—The secondary structural elements of TftD around the putative substrate-binding pocket were superimposable with those in available holo-form structures of the above-mentioned enzymes, MCAD (3MDE), HpaB (2YYJ), and 4-BUDH (1U8V). Therefore, a reliable position for the riboflavin moiety of $FADH_2$ could be established. However, the residues for coordinating the pyrophosphate or adenosine group of the $FAD(H_2)$ could not be pinpointed due to the conformational differences among the four subunits of apo-form TftD. The two conserved residues (Fig. 8), Gln-157 and Arg-160, which reside in the flexible loop between β5 and β6 and coordinate the phosphate group of $FADH_2$ in HpaB (36), are not in the coordination position in TftD. Therefore, upon $FADH_2$ binding, a conformational change might follow in that local area to accommodate binding of the pyrophosphate and adenosine moieties. However, considering a noticeably weaker affinity of TftD (micromolar range) for $FADH_2$ compared with that of HpaB (nanomolar range) (5) and negligible affinity for both FAD and FMN, TftD might have intrinsically poor coordination for the ADP portion of the FAD.

The geometry and several polar residues in the *si*-face of the modeled isoalloxazine ring are well conserved among TftD, MCAD (3MDE), HpaB (2YYJ), and 4-BUDH (1U8V). Thr-192 is completely conserved among all four $FADH_2$-dependent enzymes, and their corresponding hydroxyl group side chains are in ~3.0 Å distance from the N5 atom of the isoalloxazine ring (Fig. 4*C*). In addition, three other nearby residues, Arg-100, Asp-253, and Arg-438, are conserved among TftD, TcpA, and HpaB (Fig. 8). The side chain of Arg-100 has been proposed to form a hydrogen bond with the peroxy moiety of the C4a-hydroperoxy flavin intermediate and to contribute to the formation and/or stabilization of that transient intermediate (36, 50). As observed in the HpaB·FAD complex structure, the Nϵ atom of Arg-100 of TftD is located 4.8 Å from the C4a atom of the modeled isoalloxazine ring.

The K_d of HpaB for $FADH_2$ is in a nanomolar range compared with the micromolar range for FAD binding (21). This substantially higher affinity of HpaB for $FADH_2$ over FAD has been attributed to the immediate peroxidation of $FADH_2$ and its subsequent stabilization through the guanidinium side chain of Arg-100 (36). In contrast to micromolar range affinity of HpaB for FAD, our ITC data show that TftD does not have significant affinity to FAD (Fig. 5*B*). However, in a completely anaerobic setting, which does not allow the formation of FAD or FAD-peroxide, TftD shows a K_d of 1.2 μM for $FADH_2$. Therefore, there is a clear difference in flavin affinity between TftD and HpaB.

In the *si*-side of TftD, there exists a significant difference among apolar residues in the surroundings of the bound isoalloxazine ring compared with the same side of the above-mentioned flavoenzymes. Noticeably, Val-154 is unique for TftD; the amino acid at the equivalent position is a threonine in HpaB, MCAD, and 4-BUDH. In particular, the side chain of that threonine residue in MCAD and 4-BUDH is in a position to hydrogen bond with the N1 and O2 atoms of the isoalloxazine ring. Therefore, the substitution of this residue to an apolar

Downloaded from http://www.jbc.org/ at WASHBURN UNIVERSITY on March 3, 2015

amino acid in TftD can be another reason for its negligible affinity for FAD in addition to the above-mentioned poor coordination of its AMP moiety. In addition, the corresponding residue for Val-190 is threonine, histidine, and tryptophan in HpaB, 4-BUDH, and MACD, respectively. Both histidine and tryptophan are located in proximity to the riboflavin part of the attached FAD, which could reflect its tighter affinity as a cofactor in 4-BUDH and MACD. In both TftD and HpaB, $FADH_2$ is a substrate instead of a cofactor.

The residues facing the *re*-side of the isoalloxazine ring, which is presumably a 2,5-DiCHQ or TCP-binding site, are quite different among the compared enzymes, as expected from their substrate specificities. In comparison with the corresponding residues of HpaB, the residues of TftD in the *re*-side of the isoalloxazine ring are much more apolar. For example, the corresponding residues for Leu-151, Ile-205, and Val-288 are polar in HpaB. In addition there are several other noticeable differences between these two closely related flavin-dependent monooxygenases. Previously, Tyr-104 and His-142 residues in HpaB have been noticed to coordinate the hydroxyl group of its substrate, 4-hydroxyphenyl acetate, and to abstract the proton from it, respectively. The corresponding amino acids in TftD are Ala-104 and Val-151; thus, neither of these TftD residues is able to coordinate the hydroxyl group of 2,5-DiCHQ or TCP. His-289 in the putative substrate-binding site, which is located on the *re*-side of the isoalloxazine ring, is the only candidate that could coordinate the hydroxyl group or proton abstraction from the bound substrate. Establishing a hydrogen bond between the imidazole side chain of His-289 and one of the hydroxyl groups of the modeled 2,5-DiCHQ resulted in the other hydroxyl group facing toward the solvent-exposed side of the pocket (Fig. 4*C*). Our results from site-directed mutagenesis, MALLS and CD spectra confirmed that the His-289 residue is involved in catalysis. Despite the completely abolished activity toward 2,5-DiCHQ, the H289A mutant still maintains the same CD and MALLS profile and some activity but significantly decreased the k_{cat} for the oxidation of both 2,4,5-TCP and 2,4,6-TCP (about 28- and 53-fold less, respectively), and the K_m values were only slightly altered (less than 2-fold) (Table 2). Therefore, based on these enzymatic data, the hydroxyl group of both 2,4,5- and 2,4,6-TCP may face toward the solvent area in an orientation similar to the acetate group of 4-HPA, instead of being hydrogen-bonded to the imidazole of His-289 (Fig. 9*A*). In this orientation, 4-chlorine faces into the hydrophobic side, which agrees with the hydroxylation reactions occurring in the *para*-position for TCP *versus* the *ortho*-position (to the hydroxyl group) for 4-HPA. The His-289 residue is not likely involved in abstracting a proton from the phenol group of TCP; instead, it is involved in abstraction of the proton from the added hydroxyl group in the reaction intermediate, facilitating the chlorine removal and catalytic turnover (Fig. 9*A*). Consequently, the H289A mutant slows down the catalysis of TCP. However, the His-289 residue is involved in abstracting a proton from a hydroxyl group of 2,5-DiCHQ for the hydroxylation at the *ortho*-position as noticed for 4-HPA oxidation by HpaB (Fig. 9*B*). Thus, the mutant completely loses the dechlorination activity toward 2,5-DiCHQ. Therefore, we propose that the His-289 residue of TftD plays critical bifunctional roles in its unique sequential catalysis of 2,4,5-TCP and 2,5-DiCHQ.

Closing Remark

Characterizing the participating key enzymes is the prerequisite for informed and successful bioremediation of major pollutants, which will improve our understanding of the reaction mechanisms and increase our ability to remove these pollutants from the environment. Our data offer the mechanistic understanding of TftC and TftD activities. The results support that free $FADH_2$ is generated by TftC and that TftD uses this diffused $FADH_2$ to transform 2,4,5-TCP and 2,5-DiCHQ. Furthermore, the different roles of His-289 of TftD in the catalysis of 2,4,5-TCP and 2,5-DiCHQ are proposed, explaining how a monooxygenase attacks two substrates. Besides contributions to basic biochemistry, the results may facilitate bioremediation of polychlorinated phenols.

Acknowledgments—We thank C. Ralston (Berkeley Advanced Light Source, beamline 8.2.1) and T. Terwilliger (Los Alamos National Laboratory).

REFERENCES

1. Czaplicka, M. (2004) *Sci. Total Environ.* **322,** 21–39
2. McCollister, D. D., Lockwood, D. T., and Rowe, V. K. (1961) *Toxicol. Appl. Pharmacol.* **3,** 63–70
3. Kilbane, J. J., Chatterjee, D. K., Karns, J. S., Kellogg, S. T., and Chakrabarty, A. M. (1982) *Appl. Environ. Microbiol.* **44,** 72–78
4. Kellogg, S. T., Chatterjee, D. K., and Chakrabarty, A. M. (1981) *Science* **214,** 1133–1135
5. Louie, T. M., Webster, C. M., and Xun, L. (2002) *J. Bacteriol.* **184,** 3492–3500
6. Xun, L. (1996) *J. Bacteriol* **178,** 2645–2649
7. Hübner, A., Danganan, C. E., Xun, L., Chakrabarty, A. M., and Hendrickson, W. (1998) *Appl. Environ. Microbiol.* **64,** 2086–2093
8. Gisi, M. R., and Xun, L. (2003) *J. Bacteriol.* **185,** 2786–2792
9. Perry, L. L., and Zylstra, G. J. (2007) *J. Bacteriol.* **189,** 7563–7572
10. Otto, K., Hofstetter, K., Röthlisberger, M., Witholt, B., and Schmid, A. (2004) *J. Bacteriol.* **186,** 5292–5302
11. Galán, B., Díaz, E., Prieto, M. A., and García, J. L. (2000) *J. Bacteriol.* **182,** 627–636
12. Kirchner, U., Westphal, A. H., Müller, R., and van Berkel, W. J. (2003) *J. Biol. Chem.* **278,** 47545–47553
13. Malito, E., Alfieri, A., Fraaije, M. W., and Mattevi, A. (2004) *Proc. Natl. Acad. Sci. U.S.A.* **101,** 13157–13162
14. Li, L., Liu, X., Yang, W., Xu, F., Wang, W., Feng, L., Bartlam, M., Wang, L., and Rao, Z. (2008) *J. Mol. Biol.* **376,** 453–465
15. Valton, J., Fontecave, M., Douki, T., Kendrew, S. G., and Nivière, V. (2006) *J. Biol. Chem.* **281,** 27–35
16. Massey, V. (1994) *J. Biol. Chem.* **269,** 22459–22462
17. Filisetti, L., Fontecave, M., and Niviere, V. (2003) *J. Biol. Chem.* **278,** 296–303
18. Gao, B., and Ellis, H. R. (2005) *Biochem. Biophys. Res. Commun.* **331,** 1137–1145
19. Nissen, M. S., Youn, B., Knowles, B. D., Ballinger, J. W., Jun, S. Y., Belchik, S. M., Xun, L., and Kang, C. (2008) *J. Biol. Chem.* **283,** 28710–28720
20. Gibson, Q. H., and Hastings, J. W. (1962) *Biochem. J.* **83,** 368–377
21. Louie, T. M., Xie, X. S., and Xun, L. (2003) *Biochemistry* **42,** 7509–7517
22. Sucharitakul, J., Phongsak, T., Entsch, B., Svasti, J., Chaiyen, P., and Ballou, D. P. (2007) *Biochemistry* **46,** 8611–8623
23. Jeffers, C. E., Nichols, J. C., and Tu, S. C. (2003) *Biochemistry* **42,** 529–534
24. Low, J. C., and Tu, S. C. (2003) *Photochem. Photobiol.* **77,** 446–452
25. Abdurachim, K., and Ellis, H. R. (2006) *J. Bacteriol.* **188,** 8153–8159

Downloaded from http://www.jbc.org/ at WASHBURN UNIVERSITY on March 3, 2015

26. Lee, J. K., and Zhao, H. (2007) *J. Bacteriol.* **189,** 8556–8563
27. Kantz, A., Chin, F., Nallamothu, N., Nguyen, T., and Gassner, G. T. (2005) *Arch. Biochem. Biophys.* **442,** 102–116
28. Tiirola, M. A., Männistö, M. K., Puhakka, J. A., and Kulomaa, M. S. (2002) *Appl. Environ. Microbiol.* **68,** 173–180
29. Youn, B., Moinuddin, S. G., Davin, L. B., Lewis, N. G., and Kang, C. (2005) *J. Biol. Chem.* **280,** 12917–12926
30. Otwinowski, Z., and Minor, W. (1997) *Methods Enzymol.* **276,** 307–326
31. Navaza, J. (2001) *Acta Crystallogr. D. Biol. Crystallogr.* **57,** 1367–1372
32. Terwilliger, T. C. (2001) *Acta Crystallogr. D. Biol. Crystallogr.* **57,** 1755–1762
33. Jones, T. A., Zou, J. Y., Cowan, S. W., and Kjeldgaard, M. (1991) *Acta Crystallogr. A* **47,** 110–119
34. Brünger, A., Adams, P. D., Clore, G. M., DeLano, W. L., Gros, P., Grosse-Kunstleve, R. W., Jiang, J. S., Kuszewski, J., Nilges, M., Pannu, N. S., Read, R. J., Rice, L. M., Simonson, T., and Warren, G. L. (1998) *Acta Crystallogr. Sect. D. Biol. Crystallogr*. **54,** 905–921
35. Adams, P. D., Grosse-Kunstleve, R. W., Hung, L. W., Ioerger, T. R., McCoy, A. J., Moriarty, N. W., Read, R. J., Sacchettini, J. C., Sauter, N. K., and Terwilliger, T. C. (2002) *Acta Crystallogr. D Biol. Crystallogr.* **58,** 1948–1954
36. Kim, S. H., Hisano, T., Takeda, K., Iwasaki, W., Ebihara, A., and Miki, K. (2007) *J. Biol. Chem.* **282,** 33107–33117
37. Brünger, A. T., Adams, P. D., Clore, G. M., DeLano, W. L., Gros, P., Grosse-Kunstleve, R. W., Jiang, J. S., Kuszewski, J., Nilges, M., Pannu, N. S., Read, R. J., Rice, L. M., Simonson, T., and Warren, G. L. (1998) *Acta Crystallogr. D Biol. Crystallogr.* **54,** 905–921
38. Valton, J., Mathevon, C., Fontecave, M., Nivière, V., and Ballou, D. P. (2008) *J. Biol. Chem.* **283,** 10287–10296
39. Campbell, Z. T., and Baldwin, T. O. (2009) *J. Biol. Chem.* **284,** 8322–8328
40. Newman, L. M., and Wackett, L. P. (1995) *Biochemistry* **34,** 14066–14076
41. Kadiyala, V., and Spain, J. C. (1998) *Appl. Environ. Microbiol.* **64,** 2479–2484
42. Altschul, S. F., Madden, T. L., Schäffer, A. A., Zhang, J., Zhang, Z., Miller, W., and Lipman, D. J. (1997) *Nucleic Acids Res.* **25,** 3389–3402
43. Lawrence, A. D., Deery, E., McLean, K. J., Munro, A. W., Pickersgill, R. W., Rigby, S. E., and Warren, M. J. (2008) *J. Biol. Chem.* **283,** 10813–10821
44. van den Heuvel, R. H., Westphal, A. H., Heck, A. J., Walsh, M. A., Rovida, S., van Berkel, W. J., and Mattevi, A. (2004) *J. Biol. Chem.* **279,** 12860–12867
45. Holm, L., and Sander, C. (1993) *J. Mol. Biol.* **233,** 123–138
46. Martins, B. M., Dobbek, H., Cinkaya, I., Buckel, W., and Messerschmidt, A. (2004) *Proc. Natl. Acad. Sci. U.S.A.* **101,** 15645–15649
47. Kim, J. J., Wang, M., and Paschke, R. (1993) *Proc. Natl. Acad. Sci. U.S.A.* **90,** 7523–7527
48. Okai, M., Kudo, N., Lee, W. C., Kamo, M., Nagata, K., and Tanokura, M. (2006) *Biochemistry* **45,** 5103–5110
49. Kim, S. H., Hisano, T., Iwasaki, W., Ebihara, A., and Miki, K. (2008) *Proteins* **70,** 718–730
50. Torres Pazmiño, D. E., Baas, B. J., Janssen, D. B., and Fraaije, M. W. (2008) *Biochemistry* **47,** 4082–4093
51. Davis, I. W., Leaver-Fay, A., Chen, V. B., Block, J. N., Kapral, G. J., Wang, X., Murray, L. W., Arendall, W. B., 3rd, Snoeyink, J., Richardson, J. S., and Richardson, D. C. (2007) *Nucleic Acids Res.* **35,** W375–W383

Downloaded from http://www.jbc.org/ at WASHBURN UNIVERSITY on March 3, 2015

Enzyme Catalysis and Regulation:

Characterization of Chlorophenol 4-Monooxygenase (TftD) and NADH:FAD Oxidoreductase (TftC) of Burkholderia cepacia AC1100

Brian N. Webb, Jordan W. Ballinger, Eunjung Kim, Sara M. Belchik, Ka-Sum Lam, Buhyun Youn, Mark S. Nissen, Luying Xun and ChulHee Kang

J. Biol. Chem. 2010, 285:2014-2027.
doi: 10.1074/jbc.M109.056135 originally published online November 13, 2009

Access the most updated version of this article at doi: 10.1074/jbc.M109.056135

Find articles, minireviews, Reflections and Classics on similar topics on the JBC Affinity Sites.

Alerts:
- When this article is cited
- When a correction for this article is posted

Click here to choose from all of JBC's e-mail alerts

Supplemental material:
http://www.jbc.org/content/suppl/2009/11/13/M109.056135.DC1.html

This article cites 51 references, 29 of which can be accessed free at
http://www.jbc.org/content/285/3/2014.full.html#ref-list-1

Downloaded from http://www.jbc.org/ at WASHBURN UNIVERSITY on March 3, 2015